Supporting Information

On the Role of Graphene Oxide in Bifunctional Ni/MOF/rGO Composites in Electrochemical Nitrate Detection and Oxygen Evolution Reaction

Satya Lakshmi Pasarakonda[a], Srikanth Ponnada[b], Demudu Babu Gorle[c], Rapaka S Chandra Bose[d], Anjali Palariya[e], Maryam Sadat Kiai[f], Hima Bindu Gandham[a], Murugavel Kathiresan[g], Rakesh K Sharma[b]*, Annapurna Nowduri[a]*

[a]Department of Engineering Chemistry, Andhra University College of Engineering (A), Andhra University, Visakhapatnam-530003, India.

[b]Sustainable Materials and Catalysis Research Laboratory (SMCRL), Department of Chemistry, Indian Institute of Technology Jodhpur, Karwad, Jodhpur-342037, Rajasthan, India.

[c]Materials Research Centre, Indian Institute of Science, Bangalore-560012, Karnataka, India.

[d]Centre for Materials for Electronics Technology, Thrissur-680581, Kerala, India.

[e]Department of Chemistry, Jai Narayan Vyas University (New campus), Jodhpur-342005, Rajasthan-India.

[f]Center for BioNano Interactions, School of Chemistry, University College of Dublin, Belfiled, Dubline, Ireland

[g]Electro Organic & Materials Electrochemistry Division, CSIR-Central Electrochemical Research Institute, Karaikudi, 630003, Tamil Nādu, India.

Corresponding authors

1. ***[a]Prof Annapurna Nowduri**

   Department of Engineering Chemistry

   Andhra University College of Engineering (A)

   Andhra University, Visakhapatnam-530003, India

   ***[a]Email-**dr.nannapurna@andhrauniversity.edu.in,

2. ***[b]Prof. Rakesh K Sharma, FRSC**

   Sustainable Materials and Catalysis Research Laboratory (SMCRL),

   Department of Chemistry,

   Indian Institute of Technology Jodhpur,

   Jodhpur-342037, India.

   ***[b]Email:** rks@iitj.ac.in

   Webpage: http://home.iitj.ac.in/~rks/

Synthesis of graphene oxide (GO)

The graphene oxide was synthesized using Hummer's and Offerman's techniques.[54,62] In this experiment, the following ingredients were mixed and stirred in an ice bath for 30 minutes: 0.5 g of graphite, 0.5 g of $NaNO_3$, 23 mL of H_2SO_4, and 4 g of $KMnO_4$. The resulting solution was then heated in a water bath for almost two hours while being constantly stirred, producing a concentrated paste that was green in colour. After that, 40mL of water was slowly added, and the mixture was stirred while being heated to around 90°C for about an hour. Following the addition of 100 mL of water, 3 mL of H_2O_2 (30%) was gradually added until the liquid had the appropriate concentration. The colour of the solution has evolved from dark brown to a light yellowish-brown as it has matured. After that, the hot solution was filtered and repeatedly washed with 100 mL of water to lower the pH back to 7. Finally, the product was given a few hours to dry under a vacuum.

Synthesis of reduced graphene oxide (rGO)

The above-mentioned GO was mixed with a few drops of hydrogen hydrate (a reducing agent), which was then heated at 80°C for one hour. Following filtering, the reduced product was collected before centrifugation. The finished product was then dried in an oven at 120°C for 24 hours after being rinsed three times with C_2H_5OH and distilled water.

Synthesis of nickel-based metal-organic framework (Ni-MOF)

According to our previously published work, the Ni-MOF was made by dissolving 1,3,5-benzene tricarboxylic acid (1.0 mmol L^{-1}), 4,4”-bipyridine (1.0 mmol L^{-1}), and nickel (II) nitrate (1.0 mmol L^{-1}) in 40 mL of DMF, then heating the resulting mixture at 393 K for four hours. The reaction mixture was then given time to cool to room temperature. Now, solid Ni-MOF was filtered and repeatedly cleaned with DMF and ethanol. The finished product crystals were air dried for 12 hours at 333K.

Synthesis of Ni-MOF/GO composite

The Ni-MOF solution was prepared by dissolving 1.0 mM 1, 3, 5-benzenetricarboxylic acid, 1 mM 4,4-bipyridine, and 1.0 mM nickel (II) nitrate in 40 mL of DMF, followed by the addition of 100 mg of GO. The solution was sonicated, and the resultant mixture was then heated at 393 K for 4 hours before being employed. The mixture is then let to cool until it stops being heated at room temperature. After filtration, the solid Ni-MOF/GO was collected and repeatedly washed with DMF and ethanol. The finished product is air dried at 333K for 12 hours.

Synthesis of Ni-MOF/rGO composite

1.0 mmol L^{-1} of 1, 3, 5-benzene tricarboxylic acid, 1 mmol L^{-1} of 4,4-bipyridine, and 1 mM of nickel (II) nitrate were dissolved in 40 mL of DMF, and 100 mg of rGO was then added to the solution to prepare Ni-MOF/rGO. Its ability was then used to describe the Ni-MOF/rGO that was produced. The solution was then sonicated, and the resultant combination was heated at 393 K for 4 hours. The reaction mixture was then given time to cool to room temperature. The Ni-MOF/rGO product was then recovered by filtering and washed repeatedly with DMF and C_2H_5OH to get rid of any leftover impurities. The finished product is air dried at 333K for 12 hours.

Instrumentation

The prepared Ni-MOF and composite materials were initially assessed using the X-ray diffraction technique (Bruker D8 Advance Instrument). It was done using an energy dispersive x-ray source (EDX) (Hitachi SU-8010). Utilizing images taken by a Tecnai 20 G2 High Resolution Transmission Electron Microscope (HR-TEM) (FEI, The Netherlands), surface morphology investigations were conducted. Thermo Scientific's ESCALAB 250Xi, which has an Al K source (1486.6 eV), was used to do the XPS analysis. For the FTIR examination, a

Nicolet iS 20 with a grazing angle reflector was employed, and a Horiba solei was used to collect Raman spectra for the Raman analysis.

We utilised a portable computer to control the CH Instrument CHI660E electrochemical workstation for the experiments and keep track of the outcomes. Additionally, we measured using a standard three-electrode cell with a Pt wire acting as the counter/auxiliary electrode and an Ag|AgCl|KCl (3 M) solution as the reference. As a second working electrode, a 3 mm glassy carbon electrode (GCE), both bare and modified, has been used. Additionally, the DD H_2O package has all of the solutions.

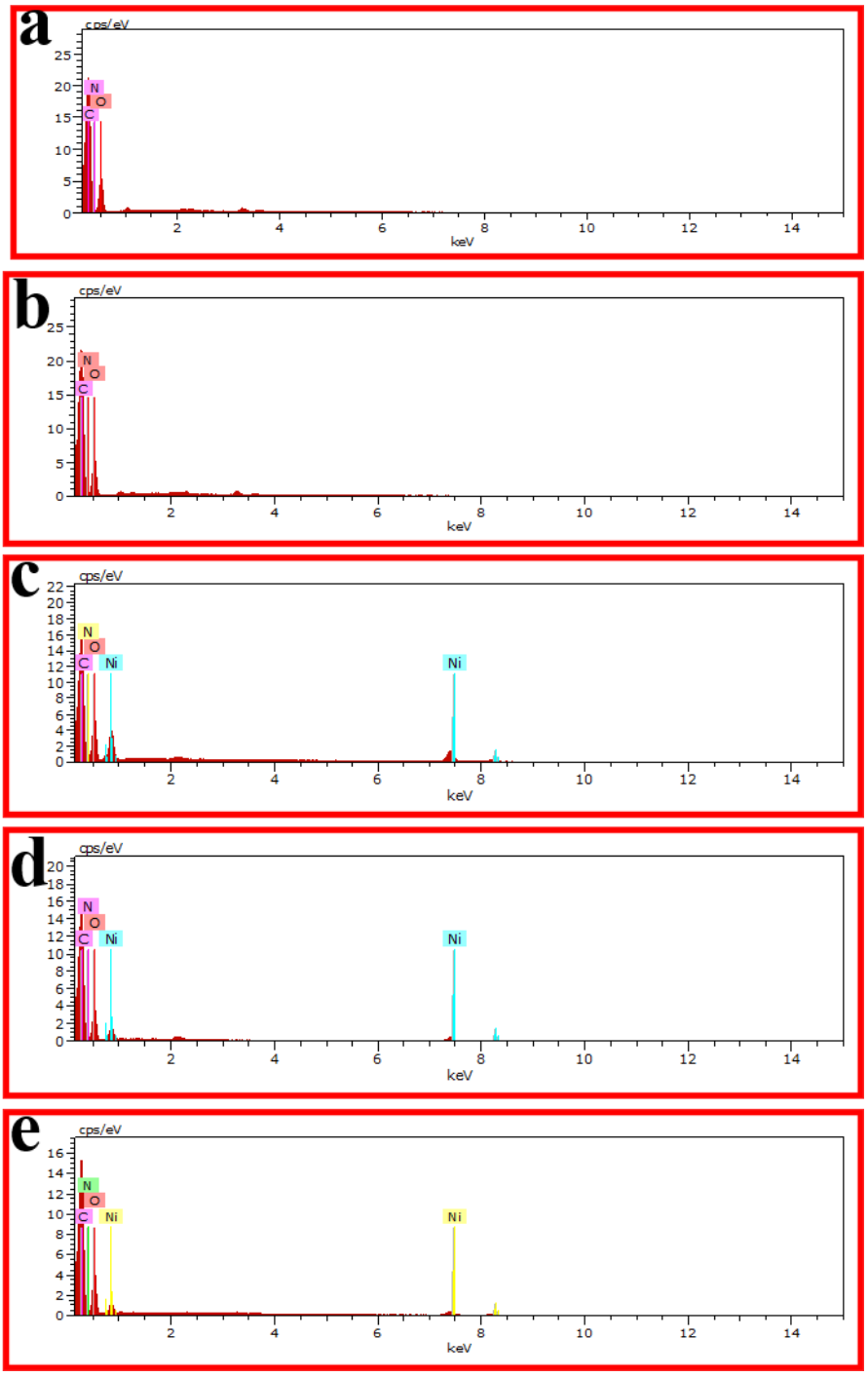

Figure S1. EDAX analysis of (a) GO, (b) rGO, (c) Ni-MOF, (d) Ni-MOG/GO, and (e) Ni-MOF/rGO.

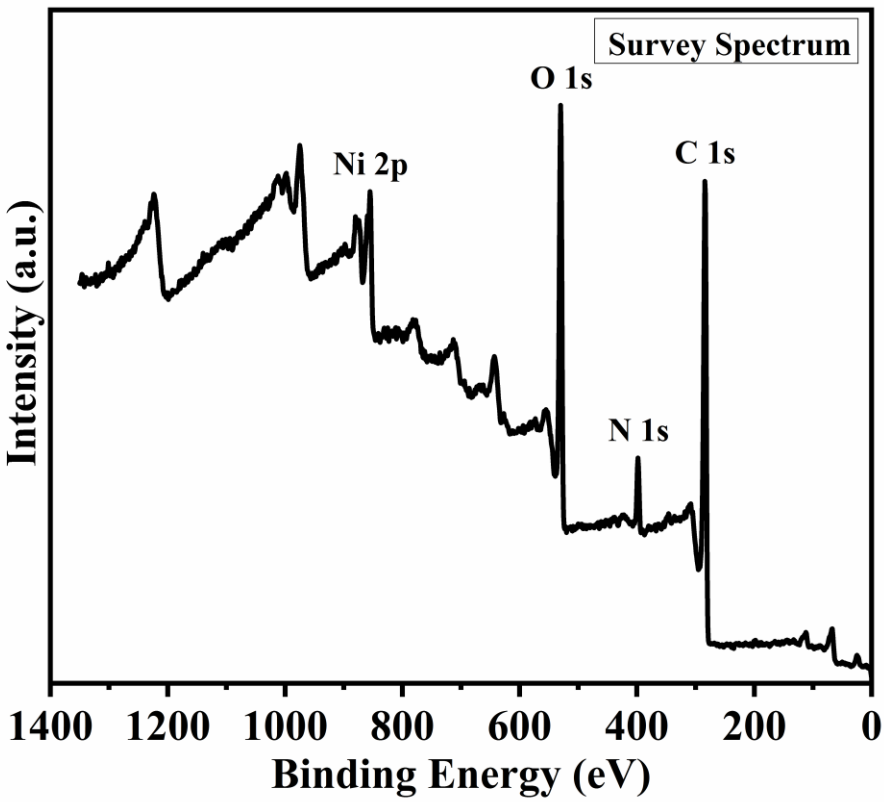

Figure S2. XPS survey spectra of Ni-MOF/rGO.

Table S1. Elemental composition of GO, rGO, Ni-MOF, Ni-MOF/GO, and Ni-MOF/rGO.

Elements	**C**		**O**		**N**		**Ni**	
Samples	**Wt%**	**At%**	**Wt%**	**At%**	**Wt%**	**At%**	**Wt%**	**At%**
GO	61.01	67.12	33.21	27.43	5.78	5.45	-	-
rGO	59.60	65.78	33.97	28.14	6.43	6.08	-	-
Ni-MOF	49.35	60.03	27.15	24.79	11.74	12.24	11.77	2.93
Ni-MOF/GO	57.18	65.28	28.28	24.24	9.51	9.31	5.03	1.17
Ni-MOF/rGO	55.67	63.55	30.50	26.14	9.50	9.30	4.33	1.01

Table S2. Comparison of the present Ni-MOF/rGO fabricated sensor with the reported sensors towards electrochemical sensing of nitrate.

Modified Electrodes	**Method**	**Linear range (µM)**	**LOD (µM)**	**Sensitivity (µA μM^{-1} cm^{-2})**	**Ref.**
NiR/rGO/PPy/GCE	CV	5×10^{3} - 10^{4}	275	-	**1**
NiR/Gr foam/Ti NF	Am	0.16-7128	0.16	42.1	**2**
NiR/ZnO NRs/AgE	Am	1-3400	1	0.45	**3**
NiR/GO/PEDOT NF/AuE	Imp	7.09-7128	2.17	3.8×10-3	**4**
NiR/nTiO_2 NFs/Gr foam	Imp	1-1000	-	0.316	**5**
GO NSh/TiE	CV	-	-	-	**6**
Gr/Cu NPs/AuE	DPV	10-90	7.89	0.20	**7**
rGO/MWCNTs/Cu NPs/GCE	SWV	0.1-75	0.02	0.215	**8**
LIG/Polyimide	Pot	$10\text{-}10^{5}$	20.6±14.8	54.8±2.5	**9**
T-f rGO/AuE	Pot	$10\text{-}10^{5}$	4	60.0±0.5	**10**
ERGO/Au NPs/GCE	Pot	$10\text{-}10^{5}$	6.30	-	**11**
L-MWCNTs/GCE	Pot	$50\text{-}10^{4}$	0.9	-	**12**
Cu NWA	LSV	10-50	9	0.0636	**13**
Cu NPs/PtE	LSV	50-1500	-	0.73	**14**
Ag NPs/AuE	SWV	0.39-50	0.39	0.1057	**15**
Ag NPs/AuE	SWV	1×10^{-3} – 0.01	9×10^{-4}	0.012	**16**
Oxide-deficient Cu-Pt	DPV	120-990	0.159	2.3782	**17**
Pd-Au NPs composite	LSV	16-242	1.19	0.29	**18**
Cu_xO-GCS/BPPGE	CV	10-100	1.032	1650	**19**
PANI/Cu NPs/GCE	LSV	$1\text{-}10^{5}$	5	0.78	**20**
PPy/graphite paste	Pot	$10\text{-}10^{5}$	<10	>52	**21**
POT-MoS2/AuE	Pot	$16\text{-}2.4\times10^{4}$	22.6	64	**22**
Ni-MOF/rGO	**DPV**	**5-10**	**4.018**	**0.08**	**This work**

WE: Working electrode, **LOD:** Limit of detection, **Am:** Amperometry, **CV:** Cyclic voltammetry, **DPV:** Differential pulse voltammetry, **SWV:** Square wave voltammetry, **LSV:** Linear Sweeping voltammetry, **GCE:** Glassy carbon electrode, **AuE:** Gold electrode, **AgE:**

Silver electrode, **TiE:** Titanium electrode, **PtE:** Platinum electrode, **BPPGE:** Basal plane pyrolytic graphite electrode, **NiR:** Nitrate reductase, **Gr:** Graphene, **GO:** Graphene oxide, **rGO:** Reduced graphene oxide, **T-*f* rGO:** Thiol- functionalized rGO, **ERGO:** Electrochemically reduced GO**, CNTs:** Carbon nanotubes, **MWCNTs:** Multiwall carbon nanotubes, **L-MWCNTs:** Lipophilic MWCNTs**, LIG:** Laser-induced graphene, **PEDOT:** poly(3,4- ethylenedioxythiophene), **PPy:** Polypyrrole, **PANI:** polyaniline, **POT-MoS2:** poly(3-octylthio- phene-2,5-diyl) - molybdenum disulfide, **ZnO:** Zinc oxide, **nTiO2:** Titanium dioxide, **CuxO-GCS:** Copper oxide impregnated glassy carbon spheres, **NF:** Nanofiber,

NWA: Nanowire array, **NR:** Nanorod, **NSh:** Nanosheet, **NP:** Nanoparticle, **M:** Measurement,

d: Day, **mth:** month, **wk:** Week, **h:** Hour.

Table S3. The results for detection of nitrate ions in bore water samples.

S. No.	**Real sample (Bore water)**	**Added (NO_3^-) (µM)**	**Deducted by our method (µM)**	**RR (%)**
1	Sample 1	5	5.235 ± 0.015	104.7
2	Sample2	5	5.312 ± 0.032	106.4
3	Sample 3	5	5.420 ± 0.021	108.4

Table S4. Comparison of the present Ni-MOF/rGO fabricated electrode with the reported electrocatalysts towards oxygen evolution reaction.

Electrocatalyst	**Electrolyte**	**Electrode**	**Over potential**	**Year**	**Ref**
1.Nickel foam and stainless-steel mesh	1 M KOH solution	GCE	0.277 V at 10 mA/cm^2	2019	23
2.Single-atom Ruthenium (Ru-N-C, nitrogen carbon support) catalyst	0.5 M H_2SO_4	GCE	0.267 V at 10 mA/cm^2	2019	24
3.Phosphorous-Doped $NiCo_2O_4$ Nanowire	1 M KOH	P-NCO NWs/NF	0.3 V at 10 mA/cm^2	2019	25
4.Metal-Free Nanoporous High-Entropy Alloys	1 M KOH	GCE	0.223 V at 10 mA/cm^2	2019	26
5.Amorphous Fe-Ni-P-B-O Nanocages	1 M KOH	GCE	0.236 V at 10 mA/cm^2	2019	27
7.Iron Nickel Catalyst	1 M KOH	Au- coated FTO	0.245 V at 10 mA/cm^2	2019	28
9.Metal-organic framework derived Co_3O_4/MoS_2 heterostructure	1 M KOH	Co_3O_4/MoS_2 foam	0.230 V at 20 mA/cm^2	2019	29
10. Fe-Doped Co- based Perovskite Oxide	0.1 M KOH	GCE	-	2019	30

11. Chromium-ruthenium oxide solid solution electrocatalyst	0.5 M H_2SO_4	GCE	0.178 V at 10 mA/cm^2	2019	31
12.$Ni_xCo_{3-x}O_4$ Electrocatalyst	1 M KOH	GCRDE	0.4 V at 10 mA/cm^2	2019	32
13. Two-Dimensional Bimetallic Nickel-cobalt Phosphate Nanoplates	1 M KOH	GCE	0.310 V at 10 mA/cm^2	2020	33
15.$CoMoO_X/CoMoS_2/CoS_x$ nanobox electrocatalysts	1 M KOH	GCE	0.281 V at 10 mA/cm^2	2020	34
16. Binder-Free Heterostructure $NiFe_2O_4$/NiFe LDH Nanosheet Composite Electrocatalysts	1 M KOH	$NiFe_2O_4$/NiFe LDH composite film	0.190 V at 100 mA/cm^2	2020	35
17. Fe doped Mo/Te nanorods	1 M KOH	GCE	0.300 V at 10 mA/cm^2	2021	36
18. Trimetallic Co-Ni-Fe oxides derived from core-shell structure metal-organic frameworks	1 M KOH	Carbon Paper electrode coated with catalyst	0.265 V at 50 mA/cm^2	2021	37
19. FeNi-based nanoparticles	1 M KOH	-	0.230 V at 10 mA/cm^2	2021	38
20. Iron doped cobalt fluoride derived CoFe layered double hydroxide	1 M KOH	GCE	0.230 V at 10 mA/cm^2	2021	39

21. High-Entropy Phosphate catalyst	1 M KOH	GCE	0.270 V at 10 mA/cm^2	2021	40
22. Hollow manganese-cobalt phosphide yolk-shell spheres	1 M KOH	GCE	0.330 V at 10 mA/cm^2	2021	41
24. IrCuNi Deeply Concave Nanocubes	0.1 M $HClO_4$	GCE	0.273 V at 10 mA/cm^2	2021	42
25. Metal-Organic Framework Derived Bimetallic NiFe Selenide Electrocatalysts	1 M KOH	CFP	0.281 V at 10 mA/cm^2	2021	43
26.NiP_2 nanosheet-implanted reduced graphene oxide composite	1 M KOH	-	0.221 V at 10 mA/cm^2	2021	44
27. Multilayer hollow $MnCo_2O_4$ microsphere	0.1 M KOH	GCE	0.340 V at 10 mA/cm^2	2021	45
28.NiCoFe-LDHs	1 M NaOH	Carbon fiber paper	0.288 V at 10 mA/cm^2	2020	46
29. Ni-MOF/rGO	**1M KOH**	**GCE**	**0.101 V at 10 mA/cm^2**	**2022**	**This work**

References

(1) Umar, M. F.; Nasar, A. Reduced graphene oxide/polypyrrole/nitrate reductase deposited glassy carbon electrode (GCE/RGO/PPy/NR): biosensor for the detection of nitrate in wastewater. *Appl. Water Sci.* **2018**, *8*, 1–10.

(2) Ali, M. A.; Mondal, K.; Wang, Y.; Mahal, N. K.; Castellano, M. J.; Dong, L. Microfluidic detection of soil nitrate ions using novel electrochemical foam electrode. *Proc. IEEE Int. Conf. Micro Electro Mech. Syst.* **2017**, *2017*, 482–485.

(3) Ahmad, R.; Bhat, K. S.; Ahn, M. S.; Hahn, Y. B. Fabrication of a robust and highly sensitive nitrate biosensor based on directly grown zinc oxide nanorods on a silver electrode. *New J. Chem.* **2017**, *41*, 10992–10997.

(4) Ali, M. A.; Jiang, H.; Mahal, N. K.; Weber, R. J.; Kumar, R.; Castellano, M. J.; Dong, L. Microfluidic impedimetric sensor for soil nitrate detection using graphene oxide and conductive nanofibers enabled sensing interface. *Sensors Actuators: B Chem.* **2017**, *239*, 1289–1299.

(5) Ali, M. A.; Jiao, Y.; Tabassum, S.; Wang, Y.; Jiang, H.; Dong, L. Electrochemical detection of nitrate ions in soil water using graphene foam modified by TiO_2 nanofibers and enzyme molecules. *Transducers* **2017**, 238–241.

(6) Ma, X.; Li, M.; Liu, X.; Wang, L.; Chen, N.; Li, J.; Feng, C. A graphene oxide nanosheetmodified Ti nanocomposite electrode with enhanced electrochemical property and stability for nitrate reduction. *Chem. Eng. J.* **2018**, *348*, 171–179.

(7) Wang, L.; Kim, J.; Cui, T. Self-assembled graphene and copper nanoparticles composite sensor for nitrate determination. *Microsyst. Technol.* **2018**, *24*, 3623–3630.

(8) Bagheri, H.; Hajian, A.; Rezaei, M.; Shirzadmehr, A. Composite of Cu metal nanoparticles-multiwall carbon nanotubes-reduced graphene oxide as a novel and high performance platform of the electrochemical sensor for simultaneous determination of nitrite and nitrate. *J. Hazard. Mater.* **2017**, *324*, 762–772.

(9) Garland, N. T.; McLamore, E. S.; Cavallaro, N. D.; Mendivelso-Perez, D.; Smith, E. A.; Jing, D.; Claussen, J. C. Flexible laser-induced graphene for nitrogen sensing in soil. *ACS Appl. Mater. Interfaces* **2018**, *10*, 39124–39133.

(10) Liu, Y.; Liu, Y.; Meng, Z.; Qin, Y.; Jiang, D.; Xi, K.; Wang, P. Thiol-functionalized reduced graphene oxide as self-assembled ion-to-electron transducer for durable solid-contact ion-selective electrodes. *Talanta* **2020**, *208*, 120374.

(11) Chen, M.; Zhang, M.; Wang, X.; Yang, Q.; Wang, M.; Liu, G.; Yao, L. An all-solid-state nitrate ion-selective electrode with nanohybrids composite films for in-situ soil nutrient monitoring. *Sensors* **2020**, *20*, 2270.

(12) Cuartero, M.; Crespo, G.; Cherubini, T.; Pankratova, N.; Confalonieri, F.; Massa, F.; Lou Tercier-Waeber, M.; Abdou, M.; Sch¨afer, J.; Bakker, E. In situ detection of macronutrients and chloride in seawater by submersible electrochemical sensors. *Anal. Chem.* **2018**, *90*, 4702–4710.

(13) Patella, B.; Russo, R. R.; O'Riordan, A.; Aiello, G.; Sunseri, C.; Inguanta, R. Copper nanowire array as highly selective electrochemical sensor of nitrate ions in water. *Talanta* **2021**, *221*, 121643.

(14) Li, Y.; Zhang, Z.; Song, Y.; Bian, C.; Sun, J.; Dong, H.; Xia, S. Determination of nitrate in potable Water using a miniaturized electrochemical sensor, in: NEMS 2018 -13th Annu. IEEE Int. Conf. Nano/Micro Eng. Mol. Syst., IEEE, **2018**, pp. 619–622.

(15) Legrand, D. C.; Barus, C.; Garçon, V. Square wave voltammetry measurements of low concentrations of nitrate using Au/AgNPs electrode in chloride solutions. *Electroanalysis* **2017**, *29*, 2882–2887.

(16) Lebon, E.; Fau, P.; Comtat, M.; Kahn, M. L.; Sournia-Saquet, A.; Temple-Boyer, P.; Dubreuil, B.; Behra, P.; Fajerwerg, K. In situ metalorganic deposition of silver nanoparticles on gold substrate and square wave voltammetry: a highly efficient combination for nanomolar detection of nitrate ions in sea water. *Chemosensors* **2018**, *6*, 1–12.

(17) Mumtarin, Z.; Rahman, M. M.; Hasnat, M. A. Electro-kinetics of conversion of NO_3^- into NO_2^- and sensing of nitrate ions via reduction reactions at copper immobilized platinum surface in the neutral medium. *Electrochim. Acta* **2020**, *346*, 135994.

(18) Zhao, S.; Tong, J.; Li, Y.; Sun, J.; Bian, C.; Xia, S. Palladium-gold modified ultramicro interdigital array electrode chip for nitrate detection in neutral water. *Micromachines* **2019**, *10*, 223.

(19) Ramakrishnappa, T.; Sureshkumar, K.; Pandurangappa, M. Copper oxide impregnated glassy carbon spheres based electrochemical interface for nitrite/nitrate sensing. *Mater. Chem. Phys.* **2020**, *245*, 122744.

(20) Essousi, H.; Barhoumi, H.; Bibani, M.; Ktari, N.; Wendler, F.; Al-Hamry, A.; Kanoun, O. Ion-imprinted electrochemical sensor based on copper nanoparticlespolyaniline matrix for nitrate detection. *J. Sensors* **2019**, *2019*, 1-14.

(21) Schwarz, J.; Trommer, K.; Mertig, M. Solid-contact ion-selective electrodes based on graphite paste for potentiometric nitrate and ammonium determinations. *Am. J. Anal. Chem.* **2018**, *9*, 591–601.

(22) Ali, M. A.; Wang, X.; Chen, Y.; Jiao, Y.; Mahal, N. K.; Moru, S.; Castellano, M. J.; Schnable, J. C.; Schnable, P. S.; Dong, L. Continuous Monitoring of Soil Nitrate Using a Miniature Sensor with Poly(3-octyl-thiophene) and Molybdenum Disulfide Nanocomposite. *ACS Appl. Mater. Interfaces* **2019**, *11*, 29195–29206.

(23) Hu, X.; Tian, X.; Lin, Y. -W.; Wang, Z. Nickel foam and stainless steel mesh as electrocatalysts for hydrogen evolution reaction, oxygen evolution reaction and overall water splitting in alkaline media. *RSC Adv.* **2019**, *9*, 31563-31571.

(24) Cao, L.; Luo, Q.; Chen, J.; Wang, L.; Lin, Y.; Wang, H.; Liu, X.; Shen, X.; Zhang, W.; Liu, W.; Qi, Z.; Jiang, Z.; Yang, J.; Yao, T. Dynamic oxygen adsorption on single-atomic Ruthenium catalyst with high performance for acidic oxygen evolution reaction. *Nat. Commun.* **2019**, *10*, 4849.

(25) Chu, W.; Shi, Z.; Hou, Y.; Ma, D.; Bai, X.; Gao, Y.; Yang, N. Trifunctional of Phosphorus-Doped NiCo2O4 Nanowire Materials for Asymmetric Supercapacitor, Oxygen Evolution Reaction, and Hydrogen Evolution Reaction. *ACS Appl. Mater. Interfaces* **2020**, *12*, 2763–2772.

(26) Qiu, H. -J.; Fang, G.; Gao, J.; Wen, Y.; Lv, J.; Li, H.; Xie, G.; Liu, X.; Sun, S. Noble Metal-Free Nanoporous High-Entropy Alloys as Highly Efficient Electrocatalysts for Oxygen Evolution Reaction. *ACS Materials Lett.* **2019**, *1*, 526–533.

(27) Ren, H.; Sun, X.; Du, C.; Zhao, J.; Liu, D.; Fang, W.; Kumar, S.; Chua, R.; Meng, S.; Kidkhunthod, P.; Song, L.; Li, S.; Madhavi, S.; Yan, Q. Amorphous Fe–Ni–P–B–O Nanocages as Efficient Electrocatalysts for Oxygen Evolution Reaction. *ACS Nano* **2019**, *13*, 12969–12979.

(28) Song, F.; Busch, M. M.; Lassalle-Kaiser, B.; Hsu, C. -S.; Petkucheva, E.; Bensimon, M.; Chen, H. M.; Corminboeuf, C.; Hu, X. An Unconventional Iron Nickel Catalyst for the Oxygen Evolution Reaction. *ACS Cent. Sci.* **2019**, *5*, 558–568.

(29) Muthurasu, A.; Maruthapandian, V.; Kim, H. Y. Metal-organic framework derived Co_3O_4/MoS_2 heterostructure for efficient bifunctional electrocatalysts for oxygen evolution reaction and hydrogen evolution reaction. *Appl. Catal. B* **2019**, *248*, 202-210.

(30) Kim, B. -J.; Fabbri, E.; Abbott, D. F.; Cheng, X.; Clark, A. H.; Nachtegaal, M.; Borlaf, M.; Castelli, I. E.; Graule, T.; Schmidt, T. J. Functional Role of Fe-Doping in Co-Based Perovskite Oxide Catalysts for Oxygen Evolution Reaction. *J. Am. Chem. Soc.* **2019**, *141*, 5231–5240.

(31) Lin, Y., Tian, Z., Zhang, L.; Ma, J.; Jiang, Z.; Deibert, B. J.; Ge, R.; Chen, L. Chromium-ruthenium oxide solid solution electrocatalyst for highly efficient oxygen evolution reaction in acidic media. *Nat. Commun.* **2019**, *10*, 162.

(32) Cui, M.; Ding, X.; Huang, X.; Shen, Z.; Lee, T. -L.; Oropeza, F. E.; Hofmann, J. P.; Hensen, E. J. M.; Zhang, K. H. L. Ni^{3+}-Induced Hole States Enhance the Oxygen Evolution Reaction Activity of $Ni_xCo_{3-x}O_4$ Electrocatalysts. *Chem. Mater.* **2019**, *31*, 7618–7625.

(33) Septiani, N. L. W.; Kaneti, Y. V.; Fathoni, K. B.; Kani, K.; Allah, A. E.; Yuliarto, B.; Nugraha.; Dipojono, H. K.; Alothman, Z. A.; Golberg, D.; Yamauchi, Y. Self-Assembly of Two-Dimensional Bimetallic Nickel–Cobalt Phosphate Nanoplates into One-Dimensional Porous Chainlike Architecture for Efficient Oxygen Evolution Reaction. *Chem. Mater.* **2020**, *32*, 7005–7018.

(34) Xu, H.; Shang, H.; Wang, C.; Jin, L.; Chen, C.; Wang, C.; Du, Y. Three-dimensional open $CoMoO_x/CoMoS_x/CoS_x$ nanobox electrocatalysts for efficient oxygen evolution reaction. *Appl. Catal. B* **2020**, *265*, 118605.

(35) Kashale, A. A.; Yi, C. -H.; Cheng, K. -Y.; Guo, J. -S.; Pan, Y. -H.; Chen, I. -W. P. Binder-Free Heterostructured $NiFe_2O_4$/NiFe LDH Nanosheet Composite Electrocatalysts for Oxygen Evolution Reactions. *ACS Appl. Energy Mater.* **2020**, *3*, 10831–10840.

(36) He, R.; Li, M.; Qiao, W.; Feng, L. Fe doped Mo/Te nanorods with improved stability for oxygen evolution reaction. *Chem. Eng. J.* **2021**, *423*, 130168.

(37) Chen, C.; Tuo, Y.; Lu, Q.; Lu, H.; Zhang, S.; Zhou, Y.; Zhang, J.; Liu, Z.; Kang, Z.; Feng, X.; Chen, D. Hierarchical trimetallic Co-Ni-Fe oxides derived from core-shell structured metal-organic frameworks for highly efficient oxygen evolution reaction. *Appl. Catal. B* **2021**, *287*, 119953.

(38) Gu, X.; Liu, Z.; Li, M.; Tian, J.; Feng, L. Surface structure regulation and evaluation of FeNi-based nanoparticles for oxygen evolution reaction. *Appl. Catal. B* **2021**, *297*, 120462.

(39) Li, M.; Gu, Y.; Chang, Y.; Gu, X.; Tian, J.; Wu, X.; Feng, L. Iron doped cobalt fluoride derived from CoFe layered double hydroxide for efficient oxygen evolution reaction. *Chem. Eng. J.* **2021**, *425*, 130686.

(40) Qiao, H.; Wang, X.; Dong, Q.; Zheng, H.; Chen, G.; Hong, M.; Yang, C. -P.; Wu, M.; He, K.; Hu, L. A high-entropy phosphate catalyst for oxygen evolution reaction. *Nano Energy* **2021**, *86*, 106029.

(41) Kaneti, Y. V.; Guo, Y.; Septiani, N. L. W.; Iqbal, M.; Jiang, X.; Takei, T.; Yuliarto, B.; Alothman, Z. A.; Golberg, D.; Yamauchi, Y. Self-templated fabrication of hierarchical hollow manganese-cobalt phosphide yolk-shell spheres for enhanced oxygen evolution reaction. *Chem. Eng. J.* **2021**, *405*, 126580.

(42) Liu, D.; Lv, Q.; Lu, S.; Fang, J.; Zhang, Y.; Wang, X.; Xue, Y.; Zhu, W.; Zhuang, Z. IrCuNi Deeply Concave Nanocubes as Highly Active Oxygen Evolution Reaction Electrocatalyst in Acid Electrolyte. *Nano Lett.* **2021**, *21*, 2809–2816.

(43) Guo, Y.; Zhang, C.; Zhang, J.; Dastafkan, K.; Wang, K.; Zhao, C.; Shi, Z. Metal–Organic Framework-Derived Bimetallic NiFe Selenide Electrocatalysts with Multiple Phases for Efficient Oxygen Evolution Reaction. *ACS Sustainable Chem. Eng.* **2021**, *9*, 2047–2056.

(44) Luo, S.; Wang, R.; Hei, P.; Gao, L.; Yang, J.; Jiao, T. Self-assembled Ni_2P nanosheet-implanted reduced graphene oxide composite as highly efficient electrocatalyst for oxygen evolution reaction. *Colloids Surf. A: Physicochem. Eng. Asp.* **2021**, *612*, 125992.

(45) Zeng, K.; Li, W.; Zhou, Y.; Sun, Z.; Lu, C.; Yan, J.; Choi, J. -H.; Yang, R. Multilayer hollow $MnCo_2O_4$ microsphere with oxygen vacancies as efficient electrocatalyst for oxygen evolution reaction. *Chem. Eng. J.* **2021**, *421*, 127831.

(46) Zhang, M.; Liu, Y.; Liu, B.; Chen, Z.; Xu, H.; Yan, K. Trimetallic NiCoFe-Layered Double Hydroxides Nanosheets Efficient for Oxygen Evolution and Highly Selective Oxidation of Biomass-Derived 5-Hydroxymethylfurfural. *ACS Catal.* **2020**, *10*, 5179–5189.